Chemical Engineering Journal 150 (2009) 49–54

Contents lists available at ScienceDirect

Chemical Engineering Journal

journal homepage: www.elsevier.com/locate/cej

Application of H-titanate nanofibers for degradation of Congo Red in an annular slurry photoreactor

Meng Nan Chong [a,b], Bo Jin [a,b,c,*], H.Y. Zhu [d], C.W.K. Chow [c], Chris Saint [b,c]

[a] School of Chemical Engineering, The University of Adelaide, Adelaide, SA 5000, Australia
[b] School of Earth and Environmental Sciences, The University of Adelaide, SA 5000, Australia
[c] Australian Water Quality Centre, SA Water Corporation, Bolivar, SA 5110, Australia
[d] School of Physical and Chemical Sciences, Queensland University of Technology, Brisbane, QLD 4001, Australia

ARTICLE INFO

Article history:
Received 16 September 2008
Received in revised form
24 November 2008
Accepted 2 December 2008

Keywords:
TiO_2
Nanofibers
Congo Red
Annular reactor
Photocatalysis
Degradation

ABSTRACT

Anatase nanofibers (TiO_2–N) were synthesized as photocatalyst for the application in an annular slurry photoreactor (ASP). The unique properties of TiO_2–N have facilitated its high reactivity and suitability for water treatment. The influence of operational variables: TiO_2–N loading, pH, aeration rate and dye concentration on the photo-degradation kinetics and efficiency to remove a model compound of Congo Red (CR) were investigated. The photo-degradation kinetics of CR followed the Langmuir–Hinshelwood regime at lower pH. The Langmuir adsorption constant, K_{L-H} was determined as 7.695×10^2 dm^3 mol^{-1}. The optimal photo-degradation rate of 3.47×10^{-2} mol dm^{-3} min^{-1} was achieved at 60 ppm CR, pH 3, aeration rate of 5 dm^3 min^{-1} and TiO_2–N loading of 4 g dm^{-3}. Batch settling tests based on Kynch's theory revealed that the TiO_2–N photocatalysts could produce a settling velocity of 8.38×10^{-4} ms^{-1}. It was expected that these novel TiO_2–N particles can deliver a true engineering solution as an industrial process for photocatalytic water treatment.

1. Introduction

Water remediation employing semiconductor titanium dioxide (TiO_2) photocatalysts has been widely regarded as the "*ideal*" and eco-sustainable solution to current water practices [1–7]. The highly reactive oxygen species (ROS) generated as a result of the photo-induced charge separation in TiO_2 particles can mineralise toxic and recalcitrant organic compounds without creating any secondary pollution [3]. To date, the commercialisation of such water abatement technology is still impeded by a series of technical challenges. The separation of the TiO_2 particles after water treatment (post separation) remains as the major problem for scaling up such a novel technology into an industrial process. This is owing to the fine particle size of the commercially available TiO_2 particles (i.e. 10–30 nm) and its tendency to agglomerate under such particle size range that reduced its practicality [3,4].

Numerous researches have been devoted in search of suitable strategies to alleviate the post separation problem. Immobilisation of the fine TiO_2 particles onto a range of larger support materials is one of a few solutions that have been examined. The immobiliser materials used include Rashig rings, stainless steel, ferromagnetic materials, different types of clay mineral, glass matrix, fiber optics and synthetic membranes [5–10]. Although such immobilising techniques ease the TiO_2 downstream separation, various scientific issues associated with such techniques need special attention. For instance, when the immobilised layer of TiO_2 (i.e. on ferromagnetic or clay material) is subjected to high temperature processing, the impurities that present on the support materials can diffuse into the TiO_2 layer and affect its photocatalytic efficiency [11,12]. In addition, immobilising TiO_2 onto supporting materials will decrease the overall specific surface area. Such an event is highly undesirable as the photocatalysis is a surface-oriented reaction.

Continuing efforts have been made to develop alternative approaches in the fabrication of TiO_2 photocatalysts with high specificity and tailored characteristics for water treatment. In this paper, a newly synthesized anatase nanofiber (TiO_2–N) with ideal characteristics for water treatment was used for the photo-degradation of Congo Red (CR) in an annular slurry photoreactor (ASP). The TiO_2–N synthesized was measured with thickness of 40–100 nm and length up to 30 μm long. Such fibril structure of TiO_2–N is expected to be separated easily and possesses superior photocatalytic performance owing to its anatase crystal phase. The photocatalytic performance of the TiO_2–N was investigated in the ASP under different operational factors, which include the TiO_2–N

* Corresponding author at: School of Earth and Environmental Sciences, The University of Adelaide, Adelaide, SA 5005, Australia. Tel.: +61 8 8303 7056; fax: +61 8 8303 6222.
E-mail address: bo.jin@adelaide.edu.au (B. Jin).

1385-8947/$ – see front matter.
doi:10.1016/j.cej.2008.12.002

loading, pH, aeration rate and initial CR concentration. Since post separation remained a crucial step in the commercial success in using TiO_2 water treatment, numerical quantification on the degree of separation for TiO_2–N will be essential. Results from a comparison study using anatase fibers with different photocatalysts revealed that the fibers could be easily separated by sedimentation from an aqueous solution within 1 h [13]. In present study, the settling rate of the anatase fibers was numerically quantified for the first time based on Kynch's theory. The hindered settling rates under the influences of different solid TiO_2–N concentration were also estimated.

2. Materials and methods

2.1. Materials

Anatase particles (~325 mesh from Aldrich) were used as received. Nitric acid HNO_3 (AR grade, Aldrich), hydrochloric acid HCl (Labserv Pronalys Australia), sodium hydroxide NaOH (AR grade, Aldrich) and Congo Red ($C_{32}H_{22}N_6Na_2O_6S_2$, Labchem Ajax Finechem, Australia) were prepared to a designated concentration by the addition of double deionised water.

2.2. Wet chemical synthesis of H-titanate nanofibers

Hydrogen titanate nanofibers were synthesized through a hydrothermal reaction between concentrated NaOH and TiO_2 and a post-synthesis ion exchange [13]. Generally, 3 g of anatase particles (~325 mesh from Aldrich) was mixed with 80 mL of 10 M NaOH. The obtained suspensions were sonicated in an ultrasonic bath for 0.5 h and then transferred into an autoclave with a PTFE container inside. The autoclave was maintained at hydrothermal temperature of 180 °C for 48 h. The precipitate (sodium titanate nanofibers) was recovered, washed with distilled water (to remove excess NaOH), exchanged with H^+ (using a 0.1 M HCl solution) to produce hydrogen titanate nanofibers, and washed again with distilled water until pH ~7 was reached. The hydrogen titanate product was dried at 80 °C for 12 h and then calcined at 700 °C for 3 h to prepare anatase nanofibers.

Anatase TiO_2 is often regarded as the best photocatalysts for the mineralisation of organic substrates [13,14]. In this study, the anatase nanofibers obtained from sodium titanate nanofibers retained the fibril morphology of the titanates. The BET specific surface area of the anatase nanofibers was found to be 15.7 $m^2\,g^{-1}$. The resultant anatase nanofibers are shown by the SEM images in Fig. 1. The measured zeta potential using the Malvern Nano ZS Series Zetasizer (Worchestershire, UK) for the hydrogen titanate nanofibers was found to exhibit a shift towards pH 4.6 as shown in Fig. 2.

2.3. Setup of annular slurry photoreactor

The ASP, a self-designed system, was setup for this study. The ASP was fabricated using stainless steel with a 256 nm peaked UV light (11 W) positioned at the central core (*z*-axis) to ensure limited external disturbances. An air sparger with pore size of 45 μm was fitted to the conical base of the ASP for providing adequate oxygen scavengers and buoyancy force for suspending TiO_2–N particles. The purpose of the conical shape bottom is to prevent the existence of a reaction dead-zone for the TiO_2–N particles. Optional sampling ports were available at a few elevated positions to allow efficient sample collection when the reaction fluid level decreased. In-situ measurement probes for pH and dissolved oxygen were fitted for data logging during the study. All the fluid connection lines were fitted with appropriate sized Tygon tubes for a complete ASP system. The experimental setup of the ASP is shown in Fig. 3.

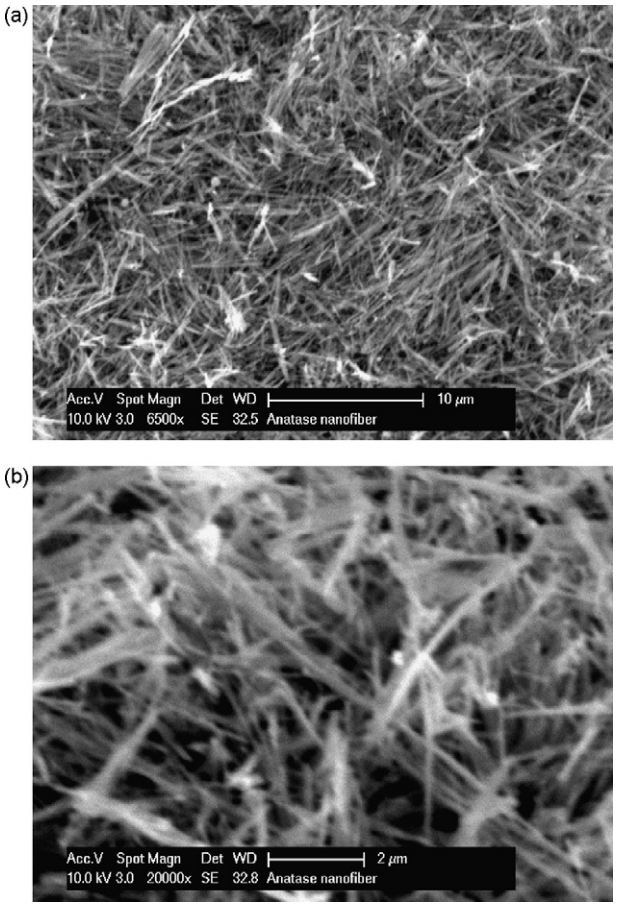

Fig. 1. SEM images for the H-titanate nanofibers at different magnifications. (a) 6500× and (b) 20,000×.

2.4. Experimental and analysis techniques

The reaction solution of CR was prepared prior to each experimental run. A specific amount of CR was first measured and mixed with the double deionised water. The pH of the solution was adjusted using sodium hydroxide (NaOH) and hydrochloric acid (HCl) as the pH corrective chemicals and a pH meter (TPS, Australia). A small flow of compressed air was allowed to run through the ASP to prevent direct sedimentation of TiO_2–N prior to the introduction of TiO_2–N/CR aqueous mixture. The compressed air flow rate was changed to the determined value once the TiO_2–N/CR aqueous mixture was added and further allowed for 0.5 h dark adsorption. The UV light was then turned on and samples were collected every 1 h for up to 6 h.

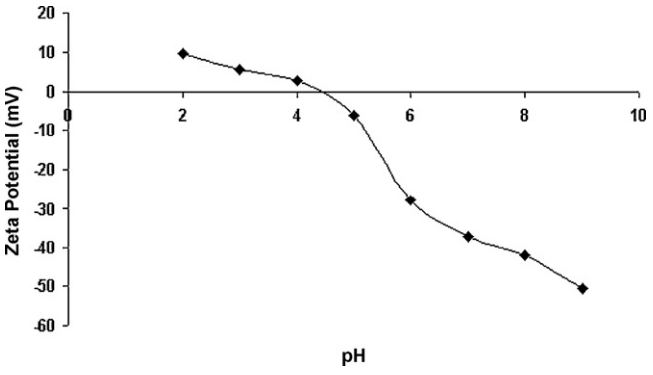

Fig. 2. Measured zeta potential for the titanate nanofibers.

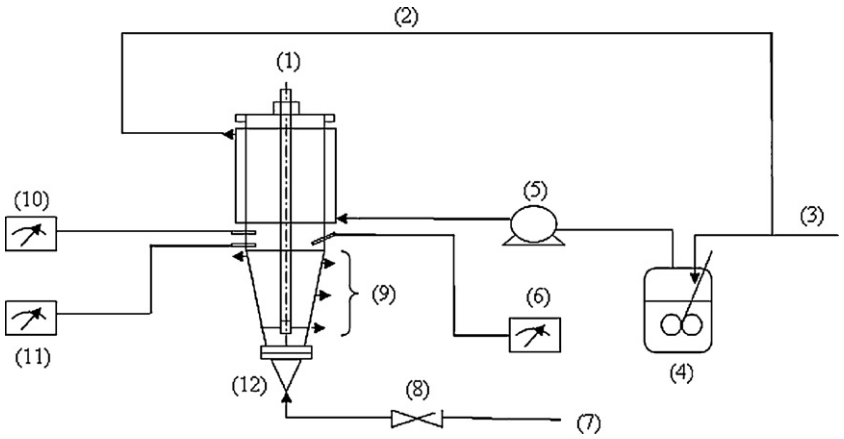

Fig. 3. Experimental setup for the annular slurry photoreactor system: (1) UV light, (2) recirculation water line, (3) fresh cool water line, (4) cooling water vessel, (5) cooling water pump, (6) temperature meter, (7) compressed air supply line, (8) compressed air regulation valve, (9) sampling ports, (10) pH meter, (11) dissolved oxygen meter and (12) photoreactor.

To analyse the CR content of the samples, monochromatic UV–vis spectrophotometer wavelength of 496.5 nm and 567 nm were employed for solution pH above 5.2 and below 3.0, respectively. The samples were centrifuged and the supernatant was decanted for analysis purpose. Prior to analysis, the samples were filtered using the Millex VX filter (Millipore 0.45 μm) to ensure the samples were free of TiO_2–N particles. The CR content of the samples was estimated from the calibration curve of the CR concentration versus absorbance intensity. Simultaneously the chemical oxygen demand (COD) for the samples was measured to compare the relationship with the spectrophotometric values using a COD measurement kit (Hach, United States). The COD measurement kit comprises of the 0–1500 ppm COD digestion solution, a Hach DRB 200 digestion chamber and a Hach DR890 COD calorimeter. Two mL of the previously filtered samples were first added into the 0–1500 ppm COD digestion solution in duplicate. All the digestion solution was then subjected to the digestion chamber at 150 °C for 120 min. After digestion, the solution was allowed to cool down prior to COD measurements using the calorimeter.

3. Results and discussion

3.1. Effects of titanate nanofiber loading

TiO_2–N loading is a crucial operational parameter, which affects significantly the removal efficiency and process cost for a photocatalysis process. Previous investigations have reported that the optimum loading for Degussa P-25 TiO_2 was in the range of 0.5–2.0 g dm^{-3}, depending on the reactor configuration and contaminant level [15,16]. In this study, the TiO_2–N loading of 0.5–4 g dm^{-3} was employed for the photo-degradation of 40 ppm CR at natural pH. Since the photo-degradation profiles exhibit a relatively linear relationship between the rates of disappearance of CR with irradiation time, a first order reaction rate model was applied. Fig. 4 shows that the kinetic profiles of different TiO_2–N loading linearly fitted well with the first order reaction rate model ($\ln C_o/C$ against reaction time). Fig. 5 shows the plot of the first order rate constant, k with its corresponding TiO_2–N loading. It could be observed that when the TiO_2–N loading was increased from 0.5 g dm^{-3} to 3.0 g dm^{-3}, the changes in the rate constant was rapid (i.e. 0.1389–0.5406 min^{-1}). However, when the TiO_2–N loading was ramped from 3.0 g dm^{-3} to 4.0 g dm^{-3}, the change in rate constant was modest from 0.5406 min^{-1} to 0.5685 min^{-1}. This trend suggested that the photo-degradation rate of CR in the ASP reached its optimal and the onset of plateau for TiO_2–N loading was approximately between 3.5 g dm^{-3} and 4.0 g dm^{-3}. The appearance of such plateau in photo-degradation rate of CR with increasing TiO_2–N loading can be attributed to the decrease in photon efficiency. As the nanofiber loading was increased, the absorption of photon by the fibers in the reaction system approached saturation. As the reaction is driven by the absorbed photons, which are one of the reactant, the saturation leads to the plateau [17–20]. Thus, a further increase in the TiO_2–N above 4.0 g dm^{-3} will not enhance the photocatalytic performance but has adverse effects on costs. Thus all the subsequent investigations on the photo-degradation of CR in the annular photoreactor had its TiO_2–N loading set at 4.0 g dm^{-3}.

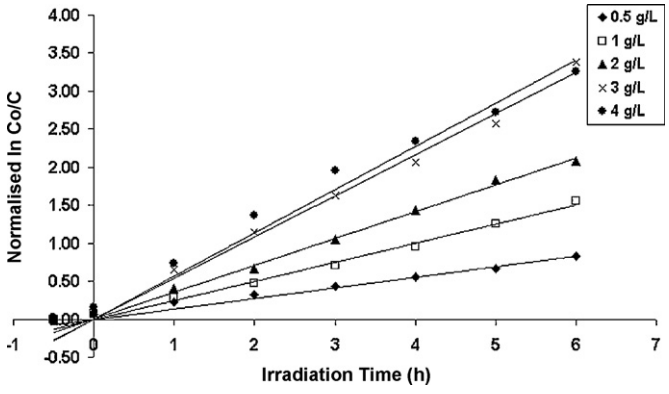

Fig. 4. First order kinetics for the photo-degradation of 40 ppm CR under different TiO_2–N loading. pH 7; aeration rate = 5 dm^3 min^{-1}. UV irradiation starts at t = 0 h.

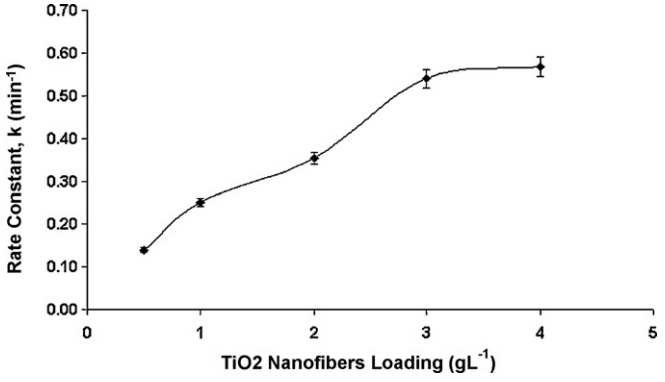

Fig. 5. Effects of TiO_2–N loading on the first order rate constant.

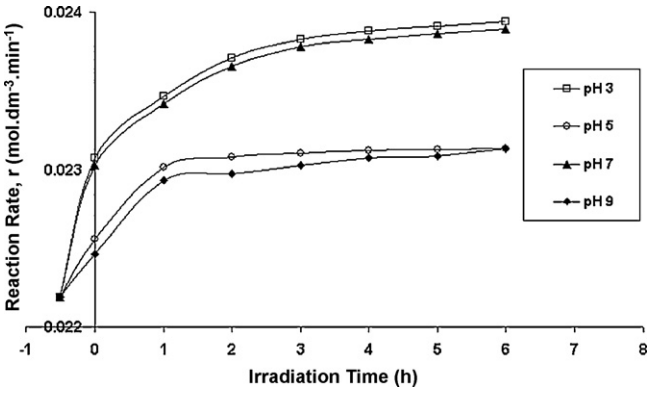

Fig. 6. Langmuir–Hinshelwood kinetic isotherms for the effects of different initial pH on its photo-degradation rate of 40 ppm CR. TiO_2–N loading of 4 g dm^{-3} and aeration rate of 5 dm^{-3} min^{-1}. UV irradiation starts at t = 0 h.

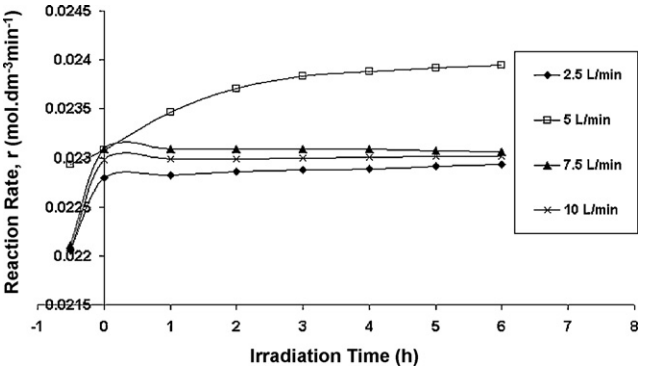

Fig. 7. Effects of different aeration rate on the photo-degradation rate of 40 ppm CR. TiO_2–N loading of 4 g dm^{-3} and pH 3. UV irradiation starts at t = 0 h.

3.2. Effects of pH

Quantifying the effects of different solution pH for the application of TiO_2–N in water treatment is of practical importance [17,18]. This is because the pH of the water in the treatment plants will have a pH range of 5.5–8.3. By knowing the photocatalytic performance of the fibers under different pH, the photo-degradation rate of CR can be predicted. In this study, the photo-degradation of CR in the ASP under different initial pH conditions (i.e. pH 3, 5, 7 and 9) were investigated. When the pH was altered from pH 7 to pH 3, it could be seen that the concentration-time profile did not obey the linear first order reaction rate equation. The initial degradation rate was significantly affected by the adsorption of CR onto the surfaces of TiO_2–N. This was evidenced from the abrupt decrease in CR concentration during the 0.5 h dark adsorption period. The initial adsorption ability gradually decreased when the solution pH increased up to 9.0. Since the linearity of the first order reaction was strongly affected by initial adsorption, the conventional Langmuir–Hinshelwood (L–H) reaction model (Eq. (1)) was applied to model the photo-degradation kinetics. Fig. 6 shows the L–H model fitted photo-degradation profiles of CR in the annular photoreactor under different pH conditions.

$$r_{CR} = -\frac{d[CR]}{dt} = \frac{kK_{L-H}[CR]}{1 + K_{L-H}[CR]} \quad (1)$$

The inception of adsorption in the photocatalysis reaction is often associated with the changes in surface charge of the TiO_2–N used. This is related to the point of zero charge (PZC) for the TiO_2–N used. The PZC for TiO_2 was reported to lie in the range of 5.6–6.8, depending on both the materials and fabrication method used to synthesize the TiO_2 particles [18–21]. However the PZC for titanate nanofibers was found to exhibit an acidic shift to pH lower than 5 as shown in Fig. 2. The PZC is a condition where the surface charge of the TiO_2–N is zero or neutral. In the co-existence of TiO_2–N in the aqueous solution, when the pH was lower than the PZC (TiO_2–N), the TiO_2–N surface will be positively charged [20,21]. The opposite trend will be observed where the particle surface will be negatively charged when pH is higher than the PZC (TiO_2–N) [21]. This explained the strong tendency for adsorption at a low pH (i.e. pH 3) with the anionic CR model organic used. At a low pH, the positively charged TiO_2–N will create a strong electrostatic attraction force on the CR molecules. This is particularly beneficial for the photocatalysis reaction using TiO_2–N. When the pH increases, the adsorption will be gradually retarded and a small repulsive force was observed when the solution pH was at 9.0. Thus, it can be concluded that operating the ASP at a low pH will enhance the degradation efficacy for removal of 40 ppm CR in the ASP. For this reason, all subsequent investigations were conducted at the lower optimal – pH 3.

3.3. Effects of aeration rate

Since the annular photoreactor used is operated as a slurry typed reactor, the total delivered aeration rate was significant for this study. Compressed air was used as the aeration source to not only maintain adequate suspension and better mixing condition, but also provide sufficient amount of dissolved oxygen. In this study, different aeration rates varying from 2.5 dm^3 min^{-1} to 10 dm^3 min^{-1} were investigated. Based on the L–H model fitted results as shown in Fig. 7, it could be observed that the ultimate reaction rate of 0.0239 mol dm^{-3} min^{-1} was achievable for the degradation of 40 ppm CR at 5 dm^3 min^{-1}. The photo-degradation rate decreased at a high aeration rate for TiO_2–N loading of 4 g dm^{-3} and pH 3. The hypothesis for such deterioration in photo-degradation rate is owed to the aeration-induced mixing turbulences of TiO_2–N in the ASP. Since the density of the TiO_2–N is approximately 400 g cm^3, a low aeration rate (i.e. 2.5 dm^3 min^{-1}) would be insufficient to maintain the TiO_2–N particles in suspension in the ASP. The increase in the aeration rate creates turbulence of the reaction aqueous mixture, resulting in a "shadow" effect that attenuates the light distribution in the ASP [18].

In addition to the achievable optimal rate under aeration rate of 5 dm^3 min^{-1}, it is also viable to examine whether the dissolved oxygen is sufficient for the photo-mineralisation of CR. For a complete mineralisation of CR, the theoretical amount of oxygen required for 1 mol of CR corresponds to 42.5 mol of oxygen as shown in Eq. (2) [22].

$$C_{32}H_{22}N_6O_6S_2{}^{2-} + 2Na^+ + 42.5O_2 \rightarrow 32CO_2 + 11H_2O + 6NO_2 + 2SO_2 \quad (2)$$

To verify the adequacy of 5 dm^3 min^{-1} of aeration in providing dissolved oxygen, Henry's law was applied. Assuming normal atmospheric conditions, the concentration of oxygen dissolved in the air saturated water as calculated using Henry's law is 0.2768 mmol dm^{-3}. As determined by stoichiometry relation, 2.44×10^{-3} mol dm^{-3} of dissolved oxygen will be required when 40 ppm CR (i.e. 5.742×10^{-5} mol dm^{-3}) is used. Since the annular photoreactor was aerated for 6.5 h, the ideal total amount of dissolved oxygen was approximately 0.5 mol and multiplying with the gas hold-up fraction in the ASP, dissolved oxygen will be in excess for the photo-mineralisation of CR. Thus the aeration rate of 5 dm^3 min^{-1} was found sufficiently optimal in this study.

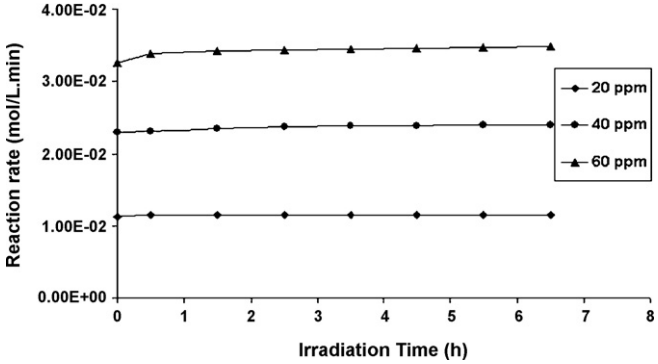

Fig. 8. Effects of different initial CR concentration on the photo-degradation rate. TiO_2–N loading of 4 g dm^{-3}, initial pH 3 and aeration rate of 5 dm^3 min^{-1}.

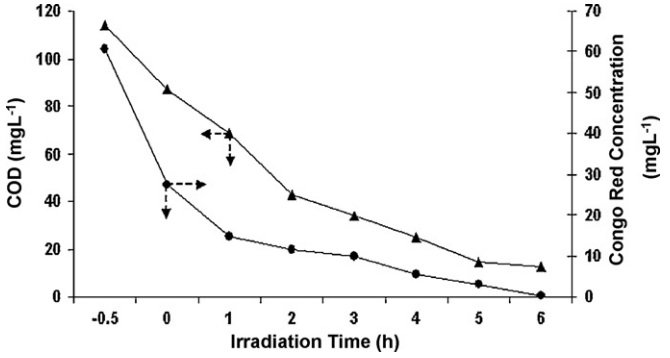

Fig. 9. Comparison for the rate of disappearance of COD against the spectrophotometric-measured CR concentration at optimum batch conditions. (TiO_2–N loading of 4 g dm^{-3}, pH 3, aeration rate of 5 dm^3 min^{-1} and initial CR concentration of 60 mg dm^{-3}). UV irradiation starts at t = 0 h.

3.4. Effects of initial Congo Red concentration

In the photocatalysis study, the reaction rate was strongly influenced by the initial amount of organic substrates present in the water matrix [23–25]. Thus the CR concentration will vary from 20 mg dm^{-3} to 60 mg dm^{-3} to visualise the ultimate effect on its photo-degradation rate. The L–H fitted kinetic isotherms for the different CR concentration were as shown in Fig. 8. To estimate the rate constant, k and Langmuir adsorption constant, $K_{L–H}$, the reciprocal plot of reaction rate against different initial CR concentration was plotted according to Eq. (3). From Eq. (3), both k and $K_{L–H}$ could be obtained from the intercept and slope of the straight line formed. It was estimated from Fig. 10 that the rate constant, k is 0.5198 min^{-1} and $K_{L–H}$ is 7.695 × 10^2 dm^3 mol^{-1}.

$$\frac{1}{R_0} = \frac{1}{k} + \frac{1}{kK_{L–H}[CR]_0} \quad (3)$$

The photo-degradation rate of CR at 60 ppm was the highest with rate equal to 3.477 × 10^{-2} mol dm^{-3} min^{-1}. Such reaction rate dictates that the TiO_2–N could degrade higher initial CR concentration with constant operating conditions of TiO_2–N loading of 4 g dm^{-3}, pH 3 and aeration rate of 5 dm^3 min^{-1}. Previous studies on photocatalytic degradation of CR have also been conducted using TiO_2 prepared from different synthesis methods [26,7,27–30]. Wahi et al. [28] prepared nine different nano-sized TiO_2 photocatalysts and found that the anatase nanorods were able to completely degrade of 14 mmol dm^{-1} in 10 h. In this study, the use of titanate nanofibers as a photocatalyst was capable to degrade 60 ppm (ca. 86 mmol dm^{-1}) of CR in 6 h of UV irradiation. This shows the anatase hydrogen titanate nanofibers as an efficient and highly potential as a photocatalyst the application in water industrial.

3.5. COD monitoring for the photo-degradation of Congo Red

Mineralisation refers to the photo-degradation of the organic compound used (i.e. CR in this study) to the innocuous final products of carbon dioxide and water. This is usually a time-consuming reaction as it involves the formation and subsequent breakdown of intermediate by-products, as a result of the hydroxylation and rupturing of the aromatic rings along the photocatalytic reaction in the annular slurry photoreactor [17].

In this study, the photo-degradation and mineralisation of CR was monitored through the measurement of both spectrophotometer and COD measurements at the optimised batch operating conditions. Fig. 9 shows the change in both the CR concentration and its corresponding COD values under the operating conditions of pH 3, of TiO_2–N loading of 4 g dm^{-3} loading, aeration rate of 5 dm^3 min^{-1} and initial CR concentration of 60 ppm. From theoretical calculation, the initial CR concentration of 60 ppm was equivalent to 117 mg L^{-1} COD from the stoichiometric relationship in Eq. (2). Fig. 9 shows that the spectrophotometric determinations of CR concentration are strongly correlated to the mineralisation of CR in terms of its COD values. Under the optimised batch operating conditions in the ASP system, a 90% reduction in COD was achievable within 6 h of irradiation time.

3.6. Kynch's analysis on titanate nanofibers

Post separation of TiO_2 particles constitutes the major challenge in photocatalytic water treatment [3]. The TiO_2–N could be separated via several methods, such as sedimentation, filtration and centrifugation. Separation by means of sedimentation is recognised as the most cost-effective method. To visualise the practicality of the newly synthesized TiO_2–N, hindered settling based on Kynch's theory was carried out in this study. This is because the particle concentrations will be high with increasing particle interactions in the majority of industrial processes [31,32]. The assumption of free particle settling condition is invalid.

In order to find the hindered settling velocity (v) of TiO_2–N, batch settling tests for the TiO_2–N have been conducted. Several TiO_2–N concentrations of 0.05 g, 0.1 g, 0.15 g and 0.2 g in 25 mL of double deionised water have been carried out. The aqueous mixture was sonicated for 15 min prior to analysis. During analysis, the change in TiO_2–N interface level with time was noted. The settling zones were distinctly seen to involve three different zones, which are the clear supernatant liquid, hindered settling zone and sediment [31,32]. The interface height (Z) measured at different time intervals for each TiO_2–N concentrations was then used to construct the settling curve, as shown in Fig. 10.

From the settling curves, the batch settling velocity could be estimated from the initial slope of the plot. It was observed that

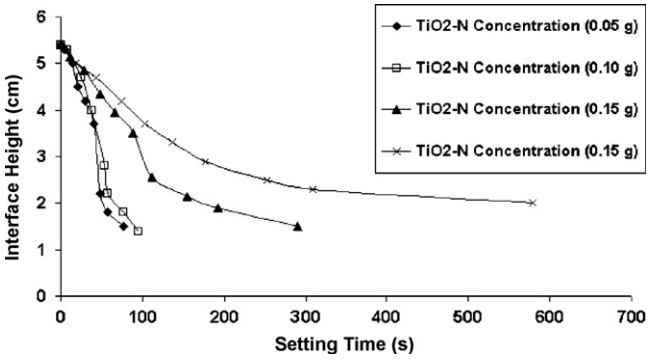

Fig. 10. Settling curves for different TiO_2–N loading in 25 mL of water.

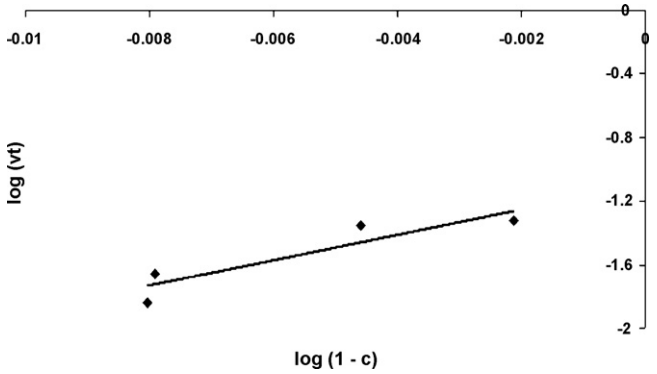

Fig. 11. Log–log plot of Richardson–Zaki correlation for single TiO_2–N terminal settling velocity.

when the TiO_2–N concentration increased, the settling velocity decreased. This is owing to the increase in overall upward flux of the water that occurs when the TiO_2–N displaces the water as it settles into the sediment zone [32]. The particle terminal velocity (v_t) could be estimated by Eq. (4), where c is the volume fraction of the TiO_2–N [32].

$$v = v_t(1 - c) \tag{4}$$

Kynch found that the instantaneous concentration at the interface of different zones do not remain constant. Instead, it is dependent on height, time and initial concentration, given by Eq. (5) [31,32].

$$c = \frac{c_0 Z_0}{Z + v_t} \tag{5}$$

$$\log(v_t) = \log(v_{t0}) + (N)\log(1 - c) \tag{6}$$

With the v_t values found for the different TiO_2–N, the linearised Richardson–Zaki correlation (i.e. Eq. (6)) is used to ultimately estimate the single particle terminal velocity v_{t0} [31,32]. Based on Fig. 11, the v_{t0} for TiO_2–N was found to be 8.38×10^{-4} m s^{-1}. This shows that the fibril morphology of TiO_2–N can facilitate the post separation sedimentation process and are highly promising for application in water treatment.

4. Conclusion

Application of anatase nanofibers for the photo-degradation of Congo Red has been demonstrated. The superior photocatalytic performance of the newly synthesized fibers in the annular slurry photoreactor has been optimised under the operating conditions of 4 g dm^{-3} anatase nanofibers loading, pH 3, and aeration rate of 5 dm^3 min^{-1}. It was interesting to note that under the same operating conditions, the rate of photo-degradation could achieve 3.47×10^{-2} mol dm^{-3} min^{-1} for 60 ppm of CR. Such reaction rate was achieved via co-adsorption of CR onto the long titanate fibers. With the specific dimensions of the anatase nanofibers, the post separation of TiO_2–N after water treatment has been resolved. The anatase nanofibers permit ease of separation, where its hindered settling rate was found to be 8.38×10^{-4} m s^{-1}. All this shows promising application of anatase nanofibers as an ideal photocatalysis in the photocatalytic water treatment.

Acknowledgement

The authors would like to thank their Honour students Ruofei Yee and Zhongde Lim for their technical assistances. This work was supported by the Australian Research Council Linkage grant (LP0562153) and the Australian Water Quality Centre, SA Water Corporation, through the Water Environmental Biotechnology Laboratory (WEBL) at the University of Adelaide.

References

[1] A. Arques, A.M. Amat, L.S. Juanes, R.F. Vercher, M.L. Marin, M.A. Miranda, Journal of Molecular Catalysis A: Chemical 271 (2007) 221–226.
[2] D. Beydoun, R. Amal, Materials Science and Engineering B 94 (1) (2002) 71–81.
[3] A. Bhattacharyya, S. Kawi, M.B. Ray, Catalysis Today 98 (2004) 431–439.
[4] Z. Ding, H.Y. Zhu, G.Q. Lu, P.F. Greenfield, Journal of Colloid and Interface Science 209 (1998) 193–199.
[5] J. Fernandez, J. Kiwi, J. Baeza, J. Freer, C. Lizama, H.D. Mansilla, Journal of Applied Catalysis B: Environmental 48 (3) (2004) 205–211.
[6] K. Mogyorosi, I. Dekany, J.H. Fendler, Langmuir 19 (2003) 2938–2946.
[7] R. Molinari, F. Pirillo, M. Falco, V. Loddo, L. Palmisano, Chemical Engineering and Processing 43 (2004) 1103–1114.
[8] S. Takeda, S. Suzuki, H. Odaka, H. Hosono, Thin Solid Films 392 (2) (2001) 338–344.
[9] Z. Xiong, Y. Xu, L. Zhu, J. Zhao, Langmuir 21 (2005) 10602–10607.
[10] W. Yan, B. Chen, S.M. Mahurin, E.W. Hagaman, S. Dai, H. Overbury, Journal of Physical Chemistry B 108 (9) (2004) 2793–2796.
[11] M.S. Lee, S.S. Hong, M. Mohseni, Journal of Molecular Catalysis A; Chemical 242 (2005) 135–140.
[12] M.N. Chong, V. Vimonses, S. Lei, B. Jin, C. Saint, C. Chow, Microporous and Mesoporous Materials 117 (2009) 233–242.
[13] H.Y. Zhu, Y. Lan, X.P. Gao, S.P. Ringer, Z.F. Zheng, D.Y. Song, J.C. Zhao, Journal of American Ceramics Society Articles 127 (2005) 6730–6736.
[14] H. Zhu, X. Gao, Y. Lan, D. Song, Y. Xi, J. Zhao, Journal of American Ceramics Society Communications 126 (2004) 8380–8381.
[15] A. Mills, S. Morris, Journal of Photochem. Photobiol A: Chem 71 (1993) 75–83.
[16] D. Chen, A.K. Ray, Water Research 32 (1998) 3223–3234.
[17] I.J. Ochuma, R.P. Fishwick, J. Wood, J.M. Winterbottom, Applied Catalysis B: Environmental 73 (2007) 259–268.
[18] S.S. Chin, T.M. Lim, K. Chiang, A.G. Fane, Chemical Engineering Journal 130 (2007) 53–63.
[19] A. Bhargava, M.F. Kabir, E. Vaisman, C.H. Langford, A. Kantzas, Industrial and Engineering Chemistry Research 43 (2004) 980–989.
[20] R.L. Pozzo, J.L. Giombi, M.A. Baltanas, A.E. Cassano, Applied Catalysis B: Environmental 38 (2002) 61–69.
[21] A.P. Toor, A. Verma, C.K. Jotshi, P.K. Bajpai, V. Singh, Dyes and Pigments 68 (2006) 53–60.
[22] S. Erdemoglu, S.K. Aksu, F. Sayilkan, B. Izgi, M. Asilturk, H. Sayilkan, F. Frimmel, S. Gucer, Journal of Hazardous Materials (2007), doi:10.1016/j.jhazmat.2007.11.087.
[23] L. Rizzo, J. Koch, V. Belgiorno, M.A. Anderson, Desalination 211 (2007) 1–9.
[24] S. Mozia, M. Toyoda, M. Inagaki, B. Tryba, A.W. Morawski, Journal of Hazardous Materials 140 (2007) 369–375.
[25] J.M. Herrmann, Catalysis Today 53 (1999) 115–129.
[26] S. Erdemoglu, S.K. Aksu, F. Sayilkan, B. Izgi, M. Asilturk, H. Sayilkan, F. Frimmel, S. Gucer, Journal of Hazardous Materials (2007), doi:10.1016/j.jhazmat. 007.11.087.
[27] C. Guillard, J. Disdier, C. Monnet, J. Dussaud, S. Malato, J. Blanco, M. Maldonado, J. Herrmann, Applied Catalysis B: Environmental 46 (2003) 319–332.
[28] R.K. Wahi, W.W. Yu, Y. Liu, M.L. Mejia, J.C. Falkner, W. Nolte, V.L. Colvin, Journal of Molecular Catalysis A: Chemical 242 (2005) 48–56.
[29] I.K. Konstantinou, T.A. Albanis, Applied Catalysis B: Environmental 49 (2004) 1–14.
[30] Y. Yang, Q. Wu, Y. Guo, C. Hu, E. Wang, Journal of Molecular Catalysis A: Chemical 225 (2005) 203–212.
[31] R.H. Perry, D.W. Green, Perry's Chemical Engineering Handbook, seventh ed., McGraw-Hill, 1997.
[32] J.F. Richardson, J.H. Harker, J.R. Backhurst, Coulson & Richardso's Chemical Engineering Volume 2, Particle Technology and Separation Processes, Butterworth-Heinemann, 2003.